

PUBLISHED IN:

JOURNAL OF COMPUTATIONAL AND THEORETICAL NANOSCIENCE,

VOL. 2, PP. 401-413 (2005).

## **Free Volume Properties of Sphingomyelin, DMPC, DPPC, and PLPC Bilayers**

M. Kupiainen, E. Falck, S. Ollila, P. Niemelä, and A. A. Gurtovenko

*Laboratory of Physics and Helsinki Institute of Physics,*

*Helsinki University of Technology, P.O. Box 1100, FI-02015 HUT, Finland*

M. T. Hyvönen

*Wihuri Research Institute, Kalliolinnantie 4, FI-00140 Helsinki,*

*Finland, and Laboratory of Physics and Helsinki Institute of Physics,*

*Helsinki University of Technology, P.O. Box 1100, FI-02015 HUT, Finland*

M. Patra and M. Karttunen

*Biophysics and Statistical Mechanics Group,*

*Laboratory of Computational Engineering,*

*Helsinki University of Technology, P.O. Box 9203, FI-02015 HUT, Finland*

I. Vattulainen

*Laboratory of Physics and Helsinki Institute of Physics,*

*Helsinki University of Technology, P.O. Box 1100, FI-02015 HUT,*

*Finland, and Memphys-Center of Biomembrane Physics,*

*Physics Department, University of Southern Denmark,*

*Campusvej 55, DK-5230 Odense M, Denmark*

(Dated: March 24, 2005)

## Abstract

Free volume pockets or voids are crucial for a variety of dynamic processes in lipid membranes. Voids facilitate the diffusion of lipid molecules in the plane of the membrane and are highly relevant for the permeation of small solutes across the membrane. We employ atomic-scale molecular dynamics simulations to study the free volume and packing properties of different lipid membrane systems, focusing on lipids commonly found in lipid rafts. We find that the free volume properties of membranes comprised of saturated (DMPC, DPPC) and diunsaturated (PLPC) phosphatidylcholine (PC) molecules have many common features, while bilayers consisting of palmitoylsphingomyelin (PSM) are distinctly different. PSM has a significantly smaller average close-packed cross-sectional area than the PCs. The free volume fraction is significantly larger in the center of a PSM bilayer than in the center of a DPPC bilayer. The opposite is true for the acyl chain and head group regions: here DPPC has a higher free volume fraction. A detailed analysis of the size, shape and orientation of voids in DPPC and PSM shows that the properties of voids are quite different in bilayers consisting of DPPC and PSM. Compared to DPPC, the number density of voids of all sizes is reduced in the head group and acyl chain regions of PSM. In the bilayer center the situation is reversed. Also the shapes and orientations of voids differ, especially in the acyl chain region. Together with recent work on DPPC/cholesterol mixtures [Falck et al., *Biophys. J.* **87**, 1076 (2004); *J. Chem. Phys.* **121**, 12676 (2004)], this article summarizes the central role of free volume in comprehending the structural properties of membrane domains rich in cholesterol and sphingomyelin.

*Key words:* lipid membrane, lipid bilayer, atomistic simulations, free volume, void, phospholipid

## I. INTRODUCTION

Cell membranes<sup>1-3</sup> and their role in the functioning of membrane proteins are currently subject to keen interest.<sup>3-7</sup> A wide range of studies suggest that lipid membranes are not just passive homogeneous interfaces surrounding cells and organelles and providing a fluid-like environment for membrane proteins. Quite the contrary, lipid membranes are complex heterogeneous bilayers characterized by a wide variety of different lipids, whose collective dynamics leads to intriguing phenomena such as the formation of nanoscale domains. These domains are receiving all the more attention, since it has been suggested that ordered domains known as *lipid rafts* are related to various important cellular functions.<sup>8</sup>

A common characteristic of rafts is that they are rich in cholesterol, sphingomyelin, and saturated or weakly unsaturated phospholipids. These molecules together give rise to ordered domains. Rafts are also believed to be associated with integral and peripheral proteins that stabilize the rafts and function together with them. Experimental studies support this idea: there are indications that rafts are involved in processes such as signal transduction, intracellular trafficking, and protein sorting.<sup>4,5,7</sup> These findings strongly suggest that the composition of domains in lipid membranes is related to the functioning of a variety of membrane proteins, which in many cases function as nano-sized molecular motors or are employed as molecular-scale sensors. The coupling of lipid membranes to nanoscale science is therefore an exceptionally exciting and topical issue, and highlights how cellular functioning emerges, in part, from the properties of cellular membranes.

Membranes are uniquely complex. The enormous number of different lipid species in membranes is a manifestation of this great complexity. The porous nature of membranes arising from the free space amidst molecules in a lipid bilayer is another. Cellular membranes are essentially porous thin sheets, containing substantial amounts of *free volume* or volume not occupied by any molecule.<sup>9</sup> Since the amount and distribution of free volume varies across the membrane, it plays a significant role in influencing or even governing a number of membrane properties. As for dynamics, free volume enables diffusion of lipids and proteins in the plane of the membrane,<sup>10</sup> diffusion of small molecules such as ubiquinone in the membrane interior,<sup>11</sup> and permeation of small molecules through the membrane.<sup>12-14</sup> As for structural features, it has been shown that the distribution of free volume affects the packing and ordering of molecules in membranes.<sup>15</sup>

It is tempting to think that voids and related packing effects also play a role to the lateral pressure profile<sup>16-18</sup> exerted by the lipids and other molecules on proteins embedded in membranes.

If the pressure profile of a lipid bilayer surrounding a protein changes considerably because of a change in the composition of the membrane, the conformation of the protein may change, thus affecting its function. Recent atomic-scale computational studies support this picture: changes in the pressure profile have been shown to affect the function of mechanosensitive channels.<sup>19</sup>

Summarizing, free volume plays a key role in a variety of cellular functions involving membranes. Detailed investigations of free volume and voids have so far been few. Experimentally, this is understandable, since it is exceedingly difficult to obtain detailed information of voids, whose sizes are typically of the order of 0.1 – 10 nm<sup>3</sup> or smaller. What is more surprising is that there are only a few simulation studies of voids.<sup>9,20,21</sup> Yet, atomic-scale simulations provide an exceptionally useful approach to gauge nano-scale phenomena in complex molecular systems such as lipid membranes.

Our objective is to characterize the free volume properties of a variety of different one-component membrane systems. We further discuss the effect of free volume and voids on structural and dynamical membrane properties. To this end, we employ atomistic molecular dynamics (MD) simulations together with novel analysis tools. We focus on pure one-component bilayers composed of a number of saturated and unsaturated phosphatidylcholine (PC) molecules, as well as sphingomyelin. Together with our previous work on mixtures of cholesterol and phospholipids,<sup>20</sup> this approach allows us to carry out a thorough and systematic comparison of lipids that are most prominent in ordered lipid domains. This study provides a framework for detailed studies of the packing properties of complex membrane systems, and could be extended to more complex membranes with proteins.

## II. ANALYZING FREE VOLUME IN MEMBRANES

### A. Discretizing Bilayers for Analysis of Free Volume and Packing Properties

We employed a technique outlined in Refs. 9 and 15 to study the free volume and packing properties of lipid bilayers. Each configuration was mapped onto three rectangular three-dimensional grids. If a grid point was located within the van der Waals radius of an atom belonging to a lipid molecule, it was considered to be occupied in the so-called lipid grid. The van der Waals radius of a given atomic group was taken to be half of the distance where the Lennard–Jones interaction potential of that atomic group with an identical atomic group is zero. The Lennard–Jones parameters

were extracted from the specification of the force field. The same grid construction procedure was repeated for water molecules. Those grid points which were unoccupied in both lipid and water grids were considered to be occupied on a grid characterizing free volume.

In the direction of the bilayer normal, the grids were defined between the points where the density of water starts to deviate from its bulk value, see Sect. IV C. The number of grid elements in each direction was chosen such that the linear size of an element was on the average 0.075 nm in all directions. We also used finer grids to ensure that the results were not influenced by the resolution.

The resulting discrete grids were used to compute quantities such as the average close-packed cross-sectional areas of lipids across the membranes, as well as average free areas and free area fractions as functions of the distance from the bilayer center along the bilayer normal. Though these quantities are useful and are employed in theories for lateral diffusion,<sup>10,22,23</sup> for example, they cannot give us detailed information about the distribution of free volume in bilayers: it is impossible to distinguish between very few large voids and numerous tiny ones. Such a distinction should be highly relevant from the point of view of, e.g., solute diffusion; unhindered motion within a substantial void is expected to differ from jumps between isolated voids. In the following we will outline how the grids described in this Section were used as starting points for, studying the detailed distribution of free volume in bilayers, i.e., the properties of voids or free volume pockets in different parts of a bilayer.

## **B. Discovering and Analyzing Voids or Free Volume Pockets**

Free volume grids were the starting points for studying the properties of voids. The technical details of how the voids were identified and characterized using a union/find algorithm<sup>24</sup> and principal component analysis (PCA)<sup>25</sup> can be found in Ref. 20.

To characterize voids, one must distinguish between *empty free volume* and *accessible free volume*.<sup>9</sup> So far we have been discussing empty free volume or all free volume outside the van der Waals radii of the atoms that are part of either lipid or water molecules. Accessible free volume is the kind of free volume relevant for solute diffusion in bilayers. It corresponds to the free volume accessible to the center-of-mass (CM) of a diffusing solute, and is obtained by adding the van der Waals radius of the diffusing solute molecule to the van der Waals radii of the atoms constituting the bilayer and solvent. We have used different solute sizes with radii  $r$  ranging between 0 and

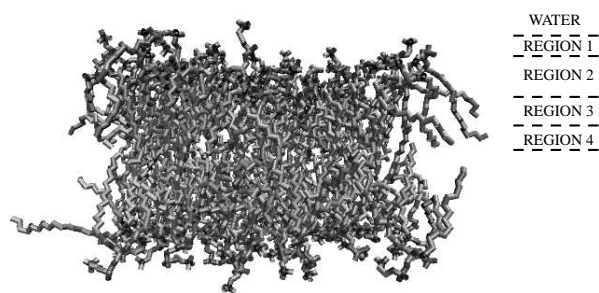


FIG. 1: Schematic illustration of regions 1 – 4 used in the analysis of voids for DPPC. The regions are shown here for the upper leaflet only. For the sake of clarity water is omitted from the presentation.

0.2 nm. These sizes are of the same magnitude as the effective van der Waals radii of, e.g., bare sodium, potassium, and chloride ions; water and oxygen molecules; and the general anesthetic xenon.

A further prerequisite for analyzing the properties of the voids is the four region model originally introduced by Marrink et al.<sup>9,26</sup> As we shall see, the free volume properties vary considerably with the position along the bilayer normal.<sup>9,15,20</sup> It is therefore not optimal to study the properties of voids averaged over the whole bilayer. Instead, we should divide the bilayer into regions with more homogeneous compositions, slightly modifying the original partition in Refs. 9 and 26. Region 1 ranges from the point where the mass density of water starts to deviate from the bulk value to the point where the densities of lipid and water are equal, see Fig. 5 (and Fig. 1). This region contains mostly water molecules and parts of lipid head groups. Region 2 extends from the point where the densities of water and lipid coincide to the point where the mass density of lipid chains exceeds  $800 \text{ kg/m}^3$ . This region is dominated by the lipid head groups, but there is also a finite density of lipid acyl chains. Region 3 is defined between the points where the mass density of lipid chains assumes the value of  $800 \text{ kg/m}^3$ . As the definition suggests, region 3 is dominated by acyl chains. The remaining part of the bilayer, i.e., the bilayer center, is region 4, with a low density of lipid chains.

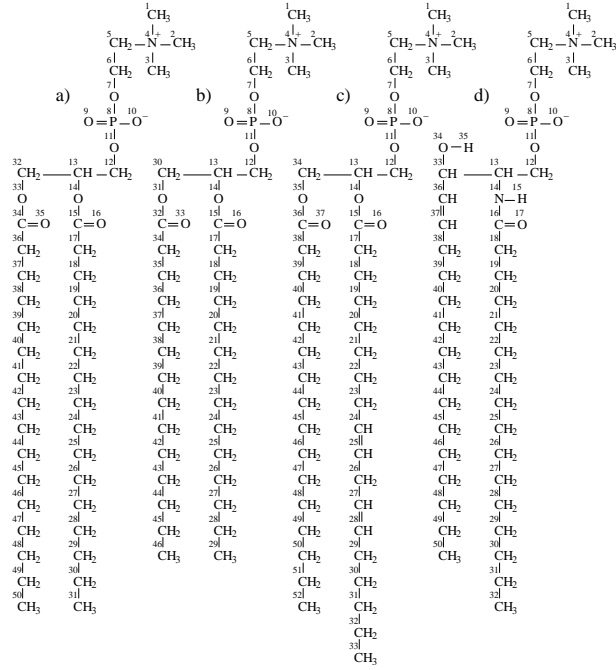


FIG. 2: Molecular descriptions of (a) DPPC, (b) DMPC, (c) PLPC, and (d) PSM molecules. The numbering shown here is used in the calculation of mass density profiles, see Table I.

### III. MD SIMULATIONS OF MEMBRANE SYSTEMS

Atomic-level molecular dynamics data for dipalmitoylphosphatidylcholine (DPPC), dimyristoylphosphatidylcholine (DMPC), and palmitoylsphingomyelin (PSM) were available from recent studies.<sup>15,27,28</sup> The sphingosine (SPH) base in PSM contains one *trans*-double bond between the 4th and 5th carbons in the SPH chain (carbons 36 and 37 in Fig. 2(d)), and its enantiomeric configuration is *D-erythro*, as is the case in nature.<sup>29</sup> The simulation data for diunsaturated 1-palmitoyl-2-linoleoyl-*sn*-glysero-3-phosphatidylcholine (PLPC)<sup>30</sup> has not been previously published (see below). Descriptions of the four molecules are shown in Fig. 2. Since most of the practical details have been discussed elsewhere, we only consider the issues most relevant for this study here.

The NpT simulations were performed using the GROMACS molecular simulation software.<sup>31</sup> All systems were comprised of 128 lipid molecules and were hydrated by 3655 water molecules. The temperature was kept constant using a Berendsen thermostat<sup>32</sup> for DMPC and DPPC simulations, and a Nosé–Hoover thermostat<sup>33,34</sup> for PSM and PLPC. In both cases, the time constant

employed was 0.1 ps. Lipid molecules and water were separately coupled to a heat bath. Pressure was controlled by a Berendsen barostat<sup>32</sup> for DMPC and DPPC, and by a Parrinello–Rahman barostat<sup>35,36</sup> for PSM and PLPC, with a time constant of 1.0 ps. The pressure coupling was applied semi-isotropically such that the sizes of the system in the  $z$  direction, i.e., in the direction of the bilayer normal, and  $xy$  plane were allowed to vary independently of each other.

For long-range electrostatic interactions we used the Particle Mesh Ewald technique,<sup>37,38</sup> which has been shown to do well in membrane simulations.<sup>39–41</sup> Water was modeled using the SPC model.<sup>42</sup> More detailed specifications for the simulations and the force fields used for these systems can be found elsewhere.<sup>15,27,28,43</sup>

The temperature used in the simulations was 323 K in all cases except for PLPC, which was simulated at 310 K. The effect of the simulation temperature to the void distribution in lipid bilayers has been discussed by Bassolino-Klimas et al.<sup>12</sup> At lower temperatures the free volume is more concentrated to the center of the bilayer, while at higher temperatures the voids in the center of the bilayer are smaller, and there are more voids in the head group region. These results should be kept in mind while analyzing the results of the PLPC simulation. Nevertheless, since all bilayers we have studied are in the liquid-disordered (fluid,  $L_\alpha$ ) phase above the main phase transition temperature, the properties we have studied here are not expected to display any major changes with the temperature.

The duration of the simulations was 100 ns for DPPC, 20 ns for DMPC, and  $\sim 50$  ns for PLPC and PSM. After equilibration of 10–20 ns, a time scale of 10–80 ns was used for analysis.

#### IV. ESSENTIAL STRUCTURAL PROPERTIES

To ensure that the bilayers have reached equilibrium and to compare them with experimental findings, we first focused on a few quantities commonly studied in experiments. These quantities are further used in Sects. V and VI to interpret the results for free volume and packing.

##### A. Equilibration

We first consider the temporal behavior of the area per lipid in the plane of the membrane,  $A(t)$ , see Fig. 3. In all PC systems equilibrium is reached within 10 ns, and in PSM within 20 ns.

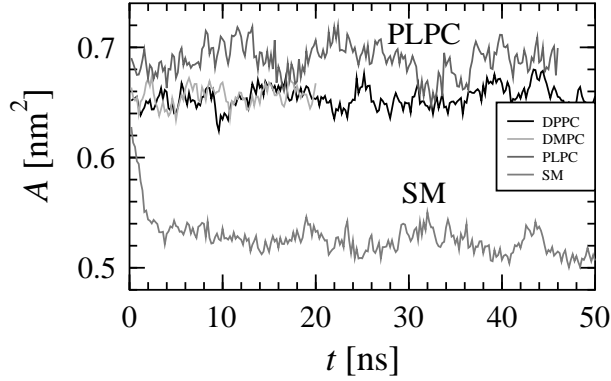


FIG. 3: Evolution of area per molecule for each system up to 50 ns. The results for DPPC and DMPC are essentially on top of each other.

Hence we have discarded this part of the data and used the remaining portion for analysis. For the average area per lipid  $\langle A \rangle$  we find  $\langle A \rangle = 0.656 \pm 0.008 \text{ nm}^2$  for DMPC,  $0.654 \pm 0.005 \text{ nm}^2$  for DPPC,  $0.689 \pm 0.009 \text{ nm}^2$  for PLPC, and  $0.527 \pm 0.008 \text{ nm}^2$  for PSM. Experimentally, results for DMPC at  $50^\circ\text{C}$  range between  $0.629 - 0.703 \text{ nm}^2$ .<sup>44-46</sup> Recent studies of DPPC point at a value of  $0.64 \text{ nm}^2$ .<sup>47</sup> For PLPC experimental results are not available, but for DOPC (dioleoylphosphatidylcholine), which has two monounsaturated chains, an experimental value  $\langle A \rangle = 0.725 \text{ nm}^2$  has been found.<sup>47</sup> Sphingomyelin systems have yielded an area per lipid  $0.47 \text{ nm}^2$  through x-ray diffraction experiments at  $328 \text{ K}$ ,<sup>48</sup> and  $0.52 \text{ nm}^2$  based on Langmuir film balance measurements at a surface pressure of  $30 \text{ mN/m}$  and  $T = 303 \text{ K}$ .<sup>49</sup> We conclude that our results are in good agreement with experiments.

## B. Ordering of Hydrocarbon Tails

Another quantity commonly measured for lipid membranes is the deuterium order parameter  $S_{\text{CD}}$ . Obtained from  $^2\text{H}$  NMR experiments, it describes the average orientational order of the lipid hydrocarbon chains with respect to the membrane normal. In simulations, one calculates the quantity

$$S_{\text{CD}} = \frac{1}{2} \langle 3 \cos^2 \theta - 1 \rangle, \quad (1)$$

where  $\theta$  is the angle between a selected C–H vector and the reference direction (bilayer normal). In a united atom simulation, the missing apolar hydrogens at their equilibrium positions can be reconstructed on the basis of the backbone chain configuration. In this work, we have reconstructed the C–H vectors and calculated the order parameters for each of them. For further discussion of

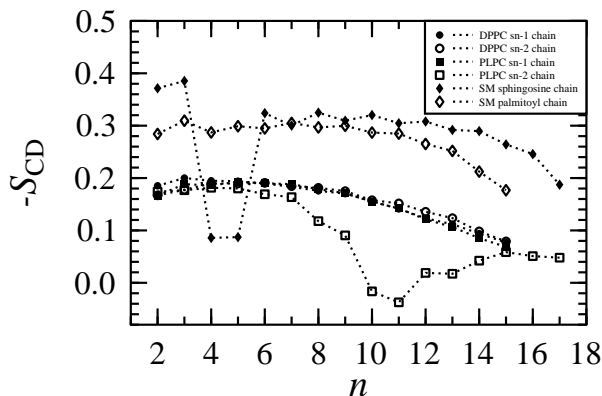


FIG. 4: Order parameters for DPPC, PLPC and PSM. Results for DMPC in Ref. 27 are not shown here. Low carbon indices  $n$  correspond to those close to the head group, and high  $n$  to those near the end of the chain.

the issue, see Refs. 28,50,51.

The order parameter profiles for DPPC, PLPC, and sphingomyelin are presented in Fig. 4. The order parameter profile of DMPC is essentially similar to that of DPPC except for the shorter chains (data not shown).

The absolute values of the deuterium order parameter for both chains of DPPC and DMPC are approximately 0.18 for  $n = 2 - 8$  and descend to 0.1 and below at the end of the tail.<sup>15,27</sup> The order parameter of the unsaturated chain of PLPC has somewhat lower order parameter values, and the variations are greater near the end of the tail. This is because of the two double bonds.<sup>43</sup> The order parameter values for sphingomyelin are considerably higher than for DPPC. The difference is typically about 0.1, except for the sphingosine chain segment for  $n = 2 - 3$ , where the values are as high as 0.4, and for  $n = 4 - 5$ , where the order parameter drops below 0.1 because of the double bond.<sup>28</sup> The high ordering and dense packing of sphingomyelin at least partly stem from the strong intermolecular hydrogen bonding discussed in Ref. 28. These results are in good agreement with experiments, see Refs. 15,27,28,39,43 and references therein.

### C. Density Profiles

The mass density profiles were first determined for the whole system, and then separately for lipids, solvent, PC head groups, and chain regions as defined in Table I. The positions of all atoms were determined with respect to the instantaneous center of mass position of the bilayer. The mass

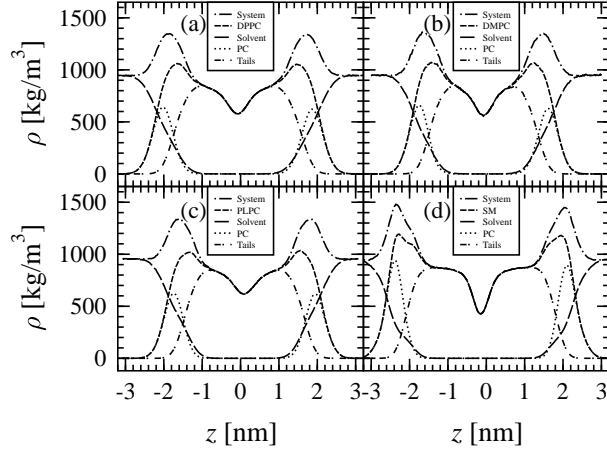


FIG. 5: Mass density profiles for (a) DPPC, (b) DMPC, (c) PLPC, and (d) sphingomyelin.

lipid	chains	PC
DPPC	12–13, 15, 17–32, 34, 36–50	1–10
DMPC	12–13, 15, 17–30, 32, 34–46	1–10
PLPC	12–13, 15, 17–34, 36, 38–52	1–10
PSM	12–13, 16, 18–33, 36–50	1–10

TABLE I: Definitions of chains (including both glycerol backbone and fatty acyl chains here) and phosphatidylcholine (PC) parts of molecules used in Fig. 5. The numbering refers to Fig. 2.

density profiles are shown in Fig. 5.

The thickness of a bilayer was defined here as the distance between the points where the mass densities of lipids and water are identical. Using this definition we found the thickness to be 3.65 nm for DMPC, 4.20 nm for DPPC, 4.08 nm for PLPC, and 4.95 nm for PSM. The thickness therefore appears to be related to the lengths and the average ordering of the hydrocarbon chains.

## V. FREE AREAS AND CLOSE-PACKED CROSS-SECTIONAL AREAS OF LIPIDS ACROSS MEMBRANES

The three-dimensional grid described in Sect. II A can be considered to be composed of a number of non-overlapping two-dimensional slices that represent the membrane at varying distances from the center of the bilayer. Pictures of these slices give a cross-sectional view of the molecular

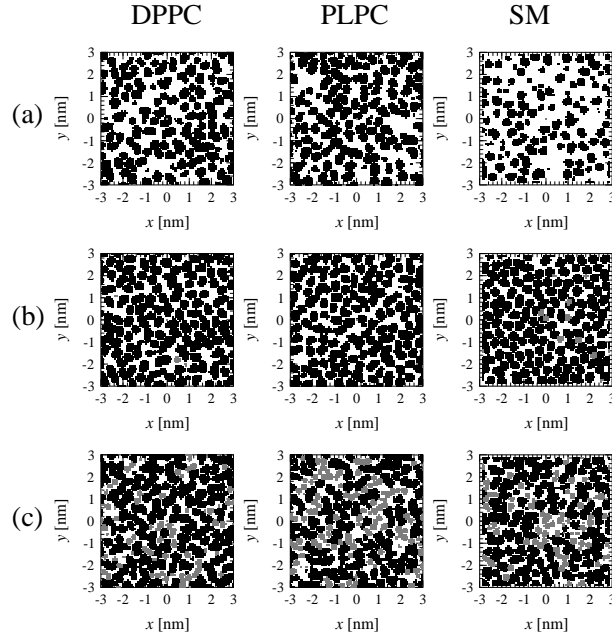


FIG. 6: Slices of lipid bilayers taken from the last configuration of each simulation. Systems in columns from left to right are DPPC, PLPC and PSM. Rows from top to bottom represent (a) the center of the bilayer at  $z = 0$ ; (b) the region where the chain's mass density peaks (according to Fig. 5,  $z = 1.0$  nm for DPPC,  $z = 0.8$  nm for PLPC, and  $z = 1.4$  nm for PSM); and (c) the region where the free area fraction has a local minimum (according to Fig. 11, for DPPC and PLPC  $z = 1.6$  nm and for PSM  $z = 2.1$  nm). The occupied lipid grid elements have been colored black, the water is gray, and the free area is white.

packing and clearly show the free area in the bilayer. Figure 6 contains examples of slices.

Slices of DMPC, DPPC, and PLPC look quite similar. There is a lot of free area in the center of the bilayer and clearly less free area in the acyl chain region. The smallest amount of free area can be found in the head group region. The slices of palmitoylsphingomyelin are somewhat different. The center of the bilayer appears to be even sparser in the case of the of PCs. At the same time, the tail and head group regions look denser than in the case of phosphatidylcholines. In the following we shall give a more quantitative view of the packing and free volume properties of the bilayers.

### A. Area Profiles

Average area profiles, i.e., the average areas occupied by lipids, solvent, as well as free areas, as functions of the distance from the bilayer center along the bilayer normal can be computed directly from the grids. In practice the area profiles are constructed by counting the area of the occupied

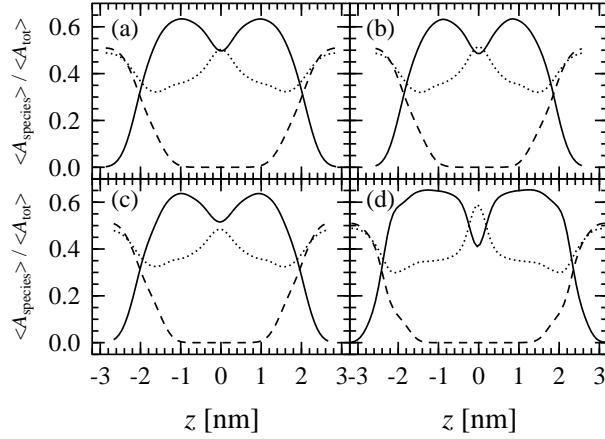


FIG. 7: Average area profiles scaled by average total bilayer area for lipid (solid line) and solvent (dashed line), as well as free area (dotted line). (a) DPPC, (b) DMPC, (c) PLPC, and (d) PSM. The errors are of the order of a few percent.

grid elements for each grid and plotting the average areas as functions of the  $z$ -coordinate, denoted by  $\langle A_{\text{species}}(z) \rangle$ . The final profiles are made by averaging over all configurations. The computed area profiles for all systems are shown in Fig. 7. The areas are scaled by the average total area  $\langle A_{\text{tot}} \rangle$ , which is obtained by multiplying the average area per lipid  $\langle A \rangle$  by the number of lipids in a monolayer.

## B. Interdigitation

To characterize interdigitation, i.e. how lipid molecules in one leaflet extend to the opposite one, we compute the number of lipid molecules in each slice. This is achieved by finding the minimum and the maximum  $z$ -coordinate of each molecule, defined by the van der Waals radii of its atoms. The molecule is considered to be present in all slices between these points. The final profile is constructed by averaging over all configurations and plotting the number of the lipids as a function of the distance from the bilayer center, see Fig. 8.

The shapes of the curves in Fig. 8 have much in common. They all have broad plateaus in the middle of the two monolayers, corresponding to the region where all 64 lipid molecules are present. All curves have a definite peak in the center of the bilayer. This peak has its origins in interdigitation of lipids. The width of the peak indicates how far to the other monolayer the lipids are extended, while the height gives the number of lipids that reach to the opposite monolayer.

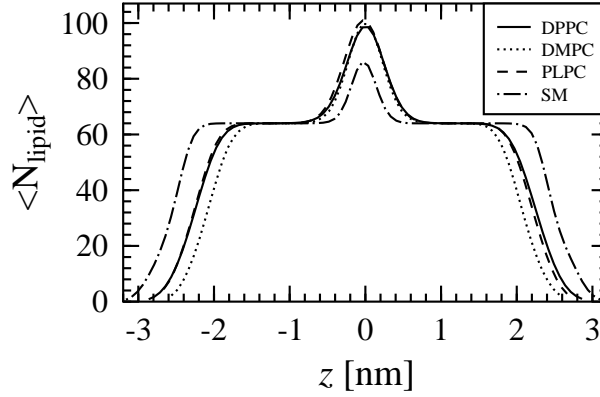


FIG. 8: Average number of lipid molecules as function of distance from bilayer center along bilayer normal. For comparison, the number of lipids in each leaflet is 64.

At the edges of the bilayer all curves decay to zero. Here a steep decay indicates a well-defined bilayer edge.

We find that 54 % of the DPPC and PLPC lipid molecules protrude to the opposite monolayer, a few of them reaching up to 0.6 nm beyond the center of the bilayer. The DMPC curve shows no significant differences from this behavior, except for the more narrow plateau region resulting of the shorter hydrocarbon chains. The fact that saturated and unsaturated PCs, as well as lipids with two chains of different lengths show no differences here is a bit surprising. This would be the case if one chain were mainly responsible of the interdigitation and the other would not play such an important role.

In the case of palmitoylsphingomyelin only 35 % of lipid molecules extend to the opposite monolayer. In addition, chains of the PSM molecules never reach more than 0.4 nm into the opposite leaflet. This is at least partly caused by the tail region of sphingomyelin being highly ordered and therefore dense: it is difficult for lipids from one monolayer to extend to the dense tail region of the other monolayer. Less interdigitation together with higher ordering of the chains result in a thicker bilayer than in the case of, e.g., DPPC, see Sect. IV C. Limited interdigitation also means less variation in the position of the molecule along the bilayer normal. This is seen as a slightly sharper edge of the PSM bilayer in Figs. 7 and 8.

The weak interdigitation found in the case of PSM is somewhat surprising, since it is commonly assumed that sphingomyelin molecules interdigitate considerably.<sup>52–54</sup> Here, however, we are dealing with palmitoylsphingomyelin, whose saturated hydrocarbon chain is short – only 16 carbons – and the chain mismatch is minor. Sphingomyelin molecules, however, come in a variety

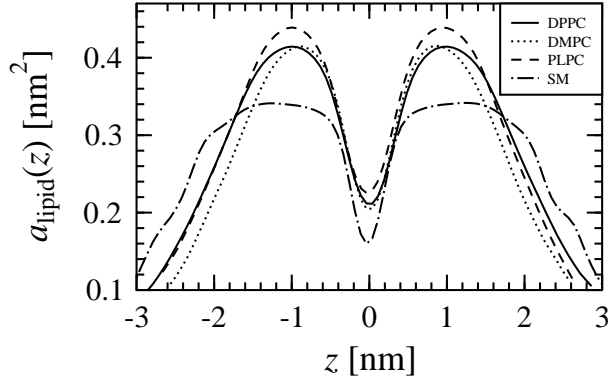


FIG. 9: Close-packed cross-sectional areas as functions of distance from bilayer center. The errors are of the order of few percent.

of different lengths: the length of the amide linked acyl chain in natural sphingomyelins varies from 16 to 24 carbons. Recent atomic-scale modeling studies suggest that interdigitation in the fluid phase becomes stronger with an increasingly long amide linked chain.<sup>55</sup> The increasing chain disparity further enhances interdigitation.

### C. Close-Packed Area Profiles

The close-packed cross-sectional area profile is a useful tool for studying the bilayer packing properties, since it reflects the space occupied by a lipid in different regions inside a membrane. A close-packed cross-sectional area profile is computed by dividing the total area occupied by lipid molecules by the average number of lipids in each slice:<sup>15</sup>

$$a_{\text{lipid}}(z) \equiv \frac{\langle A_{\text{lipid}}(z) \rangle}{\langle N_{\text{lipid}}(z) \rangle}. \quad (2)$$

The results are shown in Fig. 9.

The close-packed cross-sectional area varies considerably along the bilayer normal. In general there is a minimum in the center of the bilayer and a maximum in the acyl chain region at around 1 nm from the center. The curves for DPPC and DMPC are very similar, except that the DPPC bilayer is thicker. The close-packed area of PLPC is largely similar to that of DPPC, the main difference being the larger area of PLPC around  $z = 1.0$  nm. This is to be expected, since the double bonds should increase the cross-sectional area of a PLPC molecule.

PSM is significantly different from the phosphatidylcholines. The PSM bilayer is much thicker, which makes the profile broader and flatter. The close-packed areas differ especially in the acyl

chain region, where sphingomyelin has clearly the smallest cross-section. The more complex shape of the close-packed area in the head group region stems from the two main head group orientations in sphingomyelin, see Ref. 28. PCs only have one main head group orientation.

Comparison of close-packed area profiles to experimental data is not very easy, since experimental results for the area per lipid include both the cross-sectional close-packed area of a lipid and the average free area per lipid. What we can do is to consider values obtained from bilayers in the gel state, where the contribution of free area is as low as possible. It turns out that in DMPC bilayers in the gel state the average area per lipid is about  $0.47 \text{ nm}^2$ ,<sup>56</sup> and in DPPC  $\langle A \rangle = 0.48 \text{ nm}^2$ .<sup>47</sup> If compared with the largest cross-sectional areas in Fig. 9, the gel phase values of DMPC and DPPC (including a certain fraction of free area) are about 15 % larger than those shown in Fig. 9. As for crystal structures, an estimate for the molecular cross-sectional area of DMPC is  $0.39 \text{ nm}^2$ .<sup>57</sup> This is slightly smaller than the result in Fig. 9, as expected. Finally, Li et al. have recently conducted Langmuir monolayer experiments for palmitoylsphingomyelin monolayers.<sup>49</sup> The results suggest that the PSM layer collapses at an area per molecule of  $\sim 0.40 \text{ nm}^2$ .

#### D. Close-Packed Areas vs. Order Parameters

Petrache et al. have suggested that the deuterium order parameter and the average chain travel distance along the bilayer normal are related.<sup>58,59</sup> These ideas lead to a simple relation for deuterium order parameters and cross-sectional areas occupied by lipid molecules:

$$A_n = \frac{2A_0}{1 + \sqrt{-\frac{8}{3}\langle S_{CD}^n \rangle - \frac{1}{3}}}. \quad (3)$$

Here  $A_n$  is the cross-sectional area of a lipid molecule near segment  $n$ , and  $A_0$  is the cross-sectional area of a fully ordered lipid molecule. We can adopt a value  $A_0 \approx 0.28 \text{ nm}^2$  computed as a best fit using DPPC/cholesterol systems with a varying cholesterol concentration.<sup>15</sup>

We do not expect to be able to extract the detailed form of the close-packed area profile from the order parameters using Eq. (3). It could, however, be a useful tool for estimating the close-packed areas in the acyl chain region, i.e., at about 1 nm from the bilayer center, where the relation of close-packed cross-sectional area and the deuterium order parameter has an obvious interpretation. The value of the order parameter is computed by averaging over the tail regions for segments  $n = 3 - 8$  and over both tails, see also Sect. IV B. The close-packed areas at the distance 1 nm from the center are easily obtained from Fig. 9.

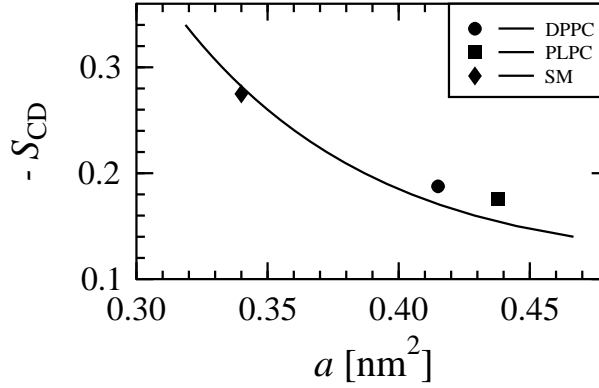


FIG. 10: Order parameters vs. close-packed areas at 1 nm from bilayer center. The solid line is plotted according to Eq. (3) and  $A_0 \approx 0.28 \text{ nm}^2$ . The result of DMPC is essentially identical with that of DPPC.

Results shown in Fig. 10 reveal that Eq. (3) gives very good results. This finding is rather surprising, since, after all, we are dealing with four different systems characterized by differences in chain length, unsaturation level, and hydrogen bonding. That despite these molecular differences we find an excellent match implies that the ordering of the hydrocarbon chains must dictate the behavior of the close-packed area in the hydrophobic membrane interior.

### E. Free Area Profiles

The free area profile is constructed by plotting the total free area in each slice divided by the number of lipids in a monolayer as a function of the  $z$ -coordinate, see Fig. 11 (a). The free area fraction, which is shown in Fig. 11 (b), is the same free area profile scaled by the average area per lipid  $\langle A \rangle$ . The two profiles demonstrate how the free volume is distributed, on the average, along the  $z$ -axis.

Each free area profile features a maximum in the center of the bilayer and a minimum in the region where the head group mass density is high, see Fig. 5. Similar shapes have been reported from modeling studies of DPPC bilayers.<sup>15,26</sup> We further find that the free area profile is inversely proportional to the mass density profile depicted in Fig. 5. This coupling is of considerable interest since, to our knowledge, there are no direct means to gauge free area profiles through experiments. The above finding suggests that, by measuring density profiles in different systems one would be able to gain better understanding of qualitative changes in free area profiles in corresponding systems.

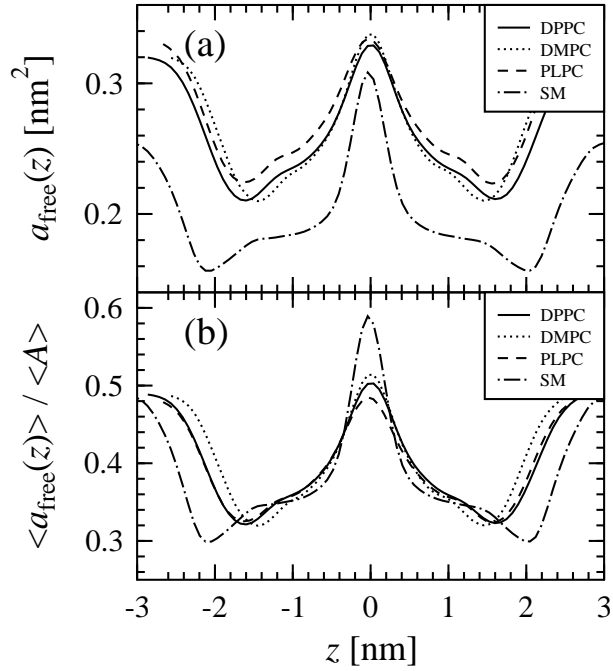


FIG. 11: Free areas per molecule as functions of distance from bilayer center. The errors are of the order of a few percent. (a) Free area per molecule and (b) the free area fraction where results in (a) have been scaled by the average area per lipid.

Naively, the shape of the profiles in Fig. 11 suggests that the movement of diffusing solutes is fastest in the center of the bilayer and that the head group region is the rate limiting step to membrane permeability. Such ideas should be taken with some caution, however, since both the distribution of small molecules inside a membrane and their partitioning into membranes depend on the subtle interplay of various interactions. For instance small molecules such as diphenylhexatriene (DPH) and pyrene commonly used as fluorescent probes do not favor the bilayer center, but are located with the acyl chains just under the head group.<sup>60–62</sup>

While the free area profiles of the different PCs do not differ significantly from each other, the PSM bilayer differs considerably from the phosphatidylcholines. Figure 11 shows that a PSM bilayer contains the least amount of free area per lipid in all parts of the bilayer. On the other hand, as Fig. 6 suggests, it has denser head group and acyl chain regions than do the PCs, but is sparser in the bilayer center.

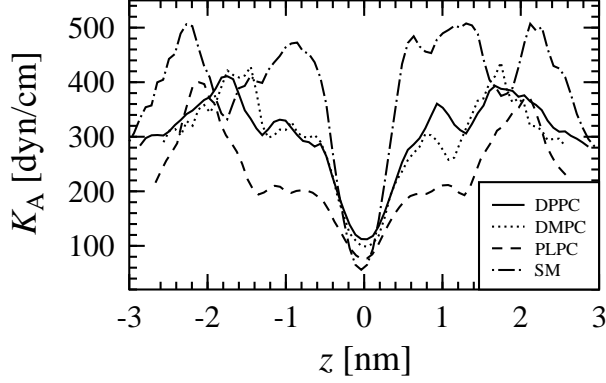


FIG. 12: Area compressibility moduli as functions of distance from bilayer center. The errors are of the order of 20 %.

### F. Area Compressibility Moduli

The lateral diffusion rates of lipid molecules depend on the amount of free volume in the bilayer; free area theories claim that a diffusion jump is not possible until there is a large enough free area next to the diffusing molecule.<sup>10,22,23</sup> The possibility of redistributing the free volume is important for diffusion. It thus seems evident that the diffusion rates depend on the magnitude of free volume fluctuations: increased fluctuations imply faster diffusion.<sup>15</sup>

The free area (or volume) fluctuations in the different regions of the bilayer can be quantified by the area compressibility modulus. The area compressibility modulus for occupied area can be defined as<sup>15</sup>

$$K_A(z) \equiv k_B T \frac{\langle A_{\text{occ}}(z) \rangle}{\langle \delta A_{\text{occ}}^2(z) \rangle}. \quad (4)$$

Here  $k_B$  is the Boltzmann constant,  $\langle A_{\text{occ}}(z) \rangle$  is the average occupied area, i.e., the area which is not free but occupied by lipid or solvent molecules, and  $\langle \delta A_{\text{occ}}^2 \rangle = \langle A_{\text{occ}}^2 \rangle - \langle A_{\text{occ}} \rangle^2$  is the variance of the occupied area. A high compressibility modulus indicates small free area fluctuations and a low compressibility modulus large fluctuations. The area compressibility moduli for DPPC, DMPC, PLPC, and PSM are shown in Fig. 12.

All compressibility moduli have a minimum in the center of the bilayer, reflecting larger fluctuations than elsewhere. Beyond this region the curves rise quickly and assume the highest values either in the acyl chain or head group region. In these regions, where the fluctuations are the smallest, spontaneous formation of reasonably sized voids necessary for diffusion jumps is not particularly likely.

Even though the error bars associated with the area compressibility moduli are reasonably large, we find that there is a significant difference between PSM and PCs especially in the acyl chain regions of the lipids. For PSM we find two different maxima located in the acyl chain region and in the vicinity of the head groups. In the case of phosphatidylcholines only the peak around the head group is present. The area compressibility data together with the free volume fraction profiles shown in Fig. 11 thus indicate that in PSM bilayers the free area and its fluctuations in the acyl chain and head group regions are more suppressed than in the systems composed of PCs. As a consequence, the lateral diffusion in PSM is considerably slower than in the other systems.<sup>28</sup>

## VI. VOIDS IN MEMBRANES

The mean-field quantities discussed so far indicate that the free volume properties of sphingomyelin are distinctly different from the phosphatidylcholines DPPC, DMPC, and PLPC. In this Section, we will compare the detailed distribution of free volume in bilayers consisting of DPPC and sphingomyelin.

### A. Void Sizes

To study void sizes we first calculated  $N(V)$ , the number of voids of a given size  $V$ , for both DPPC and sphingomyelin. These distributions were calculated separately for each of the four regions. The distributions were subsequently normalized by volume, e.g., in the case of region 4  $N(V)$  was scaled by the total volume of region 4,  $V_{R4}$ . This procedure results in a number density of voids of a given size, and facilitates comparison between DPPC and sphingomyelin. The mean-field quantities related to void number densities are the free area fractions shown in Fig. 11 (b).

The void number density distributions calculated for the four regions and using solute radii  $r \in \{0.05, 0.09, 0.12, 0.15\}$  nm are shown in Figs. 13– 16. The different  $r$  have been chosen carefully to illustrate how solutes of different sizes perceive their DPPC and sphingomyelin environments. In the case of  $r = 0.05$  nm, the accessible free volume percolates in the plane of the bilayer in both DPPC and sphingomyelin. By percolation in, e.g.,  $x$  direction, we mean that there is a large void stretching, in the  $x$  direction, from one side of the bilayer to the opposite side. For a more detailed

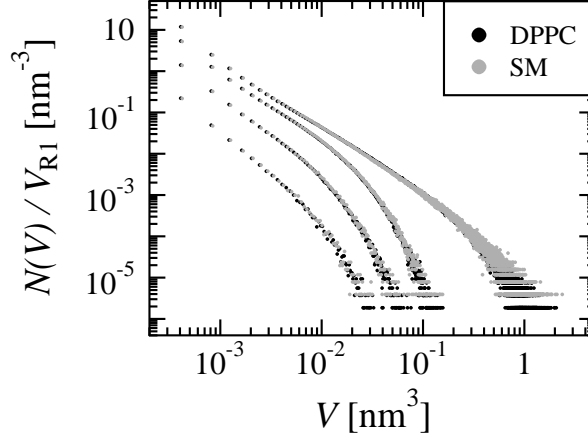


FIG. 13: Void number density distributions in region 1. The solute radii from top to bottom are  $r = 0.05$  nm,  $r = 0.09$  nm,  $r = 0.12$  nm, and  $r = 0.15$  nm. For errors, see Fig. 16.

discussion on percolation see Refs. 9,20,63. The percolating cluster of free volume is in the bilayer center, i.e., in region 4. When  $r = 0.09$  nm, there is no percolating cluster in DPPC, while the sphingomyelin bilayer still displays percolation in the plane of the bilayer in the bilayer center. This is because the free volume fraction in the bilayer center is larger in sphingomyelin than in DPPC, see Fig. 11. Finally, for  $r \in \{0.12, 0.15\}$  nm there is no percolating cluster in either DPPC or sphingomyelin. Had we chosen to study cases where  $r \lesssim 0.04$  nm, we should have observed percolation in the direction of the bilayer normal, as well. Such small solutes are, however, rather unphysical.

Figure 13 suggests that from the point of view of free volume and voids, region 1 in DPPC differs very little from the corresponding region in sphingomyelin. This is to be expected: most of region 1 consists of perturbed water. Note that also the free area fractions in DPPC and sphingomyelin are very similar in region 1, in agreement with the near-identical void number density distributions.

In case of region 2, depicted in Fig. 14, it appears that larger solutes with  $r > 0.05$  nm see, for all  $V$ , a slightly larger void number density in DPPC than in sphingomyelin. This is what one might anticipate, since the hydrogen bonding network in the head group region of a sphingomyelin bilayer should make its region 2 denser.<sup>28</sup> This is reflected at mean-field level in the free area fractions: in Region 2 the free area fraction is clearly smaller in sphingomyelin than in DPPC, see

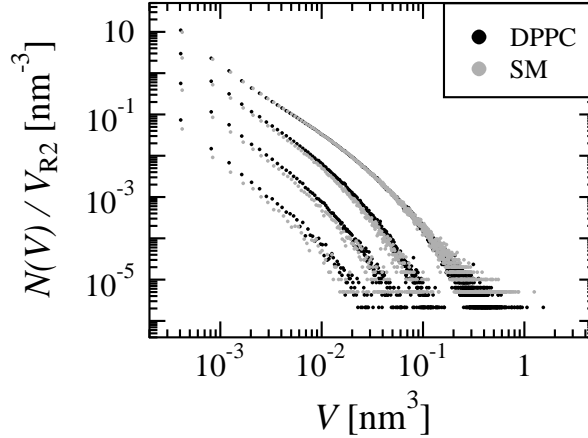


FIG. 14: Void number density distributions in region 2. The solute radii from top to bottom are  $r = 0.05$  nm,  $r = 0.09$  nm,  $r = 0.12$  nm, and  $r = 0.15$  nm. For errors, see Fig. 16.

Fig. 11. The results for  $r = 0.05$  nm, i.e., the near-identical void number densities for DPPC and sphingomyelin, most probably stem from the existence of a large percolating cluster in the bilayer center. A large percolating cluster whose center of mass is in region 4, and which therefore is assigned to region 4, may extend all the way to region 2 and thus affects the void number density distribution in region 2. As the percolating cluster is larger in DPPC than in sphingomyelin, see Fig. 14, the DPPC bilayer now looks as dense as sphingomyelin here.

As shown in Fig. 15, region 3 has certain features in common with region 2: for larger solutes with  $r > 0.05$  nm and for all  $V$ , DPPC appears to have the larger void number density of the two systems. Again, this makes sense, since the acyl chain region of sphingomyelin is more ordered, see Fig. 4, and therefore denser. The differences between DPPC and sphingomyelin are a little larger than in the case of region 2, in some cases up to a factor of five. Note that, again, the results are in agreement with the mean-field picture: in region 3 the free area fraction of DPPC is slightly larger than that of sphingomyelin. The behavior in the case of  $r = 0.05$  nm also has its origins in the large percolating cluster, which is assigned to region 4, but extends to regions 2 and 3.

The void number density distribution in region 4 is shown in Fig. 16. When  $r = 0.05$  nm the distributions for DPPC and sphingomyelin differ for larger  $V$ : DPPC appears to have slightly larger void number densities, and the percolating cluster looks a little larger than in the case of sphingomyelin. This is puzzling at first sight, since the free area fraction, see Fig. 11, is signifi-

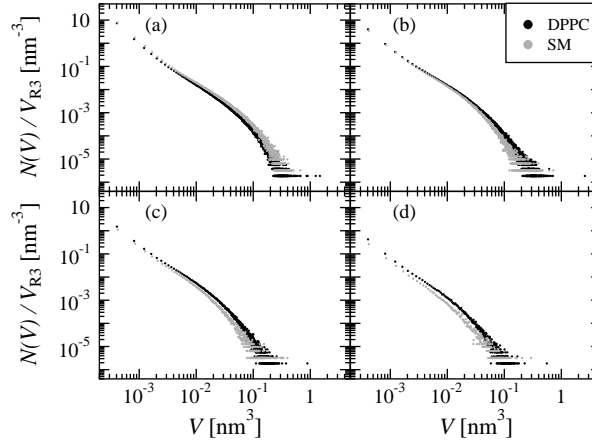


FIG. 15: Void number density distributions in region 3: (a)  $r = 0.05$  nm, (b)  $r = 0.09$  nm, (c)  $r = 0.12$  nm, and (d)  $r = 0.15$  nm. For errors, see Fig. 16.

cantly larger in sphingomyelin than in DPPC. The results can, again, be explained by the fact that the largest clusters are not truly confined to region 4, but contain free volume from regions 2 and 3, as well. As regions 2 and 3 are sparser in DPPC than in sphingomyelin, the largest clusters in region 4 appear more numerous and larger in DPPC. As  $r$  grows beyond 0.1 nm, the free volume becomes less connected, and we need no longer worry about large clusters that occupy free volume from several regions. Now the void number density distributions comply with the free area fractions: sphingomyelin has a larger void number density for all  $V$ .

Summarizing, the perturbed water regions are nearly identical in DPPC and sphingomyelin. The head group and acyl chain regions are denser, i.e., have a lower void number density, in sphingomyelin. The bilayer center is the opposite: here sphingomyelin has the largest number density of voids of all sizes.

## B. Void Shapes

Principal component analysis was used to characterize the shapes of voids with  $4 \times 10^{-3} \text{ nm}^3 < V < 0.13 \text{ nm}^3$ . As opposed to larger voids with more complicated shapes, the voids in this size range are ellipsoidal, and therefore may be characterized using PCA. PCA allows us to extract  $\sigma_1$ ,  $\sigma_2$ , and  $\sigma_3$ , which are proportional to the lengths of the principal axes of an ellipsoidal void such

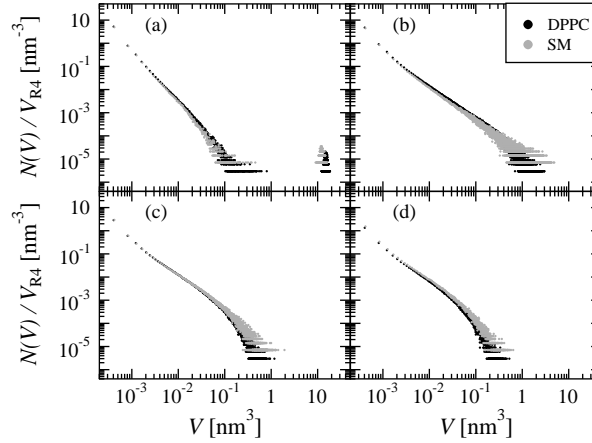


FIG. 16: Void number density distributions in region 4: (a)  $r = 0.05$  nm, (b)  $r = 0.09$  nm, (c)  $r = 0.12$  nm, and (d)  $r = 0.15$  nm. The finite statistics lead to relative errors that grow with  $V$ . For  $V < 0.01$  nm<sup>3</sup> the errors in  $N(V)/V$  are smaller than a percent, and in the range  $0.01$  nm<sup>3</sup>  $< V < 0.1$  nm<sup>3</sup> smaller than ten percent. If  $V$  is of the order of  $1$  nm<sup>3</sup>, the relative errors may be of the order of 100%. As the data are shown on a loglog scale, this is hardly a problem.

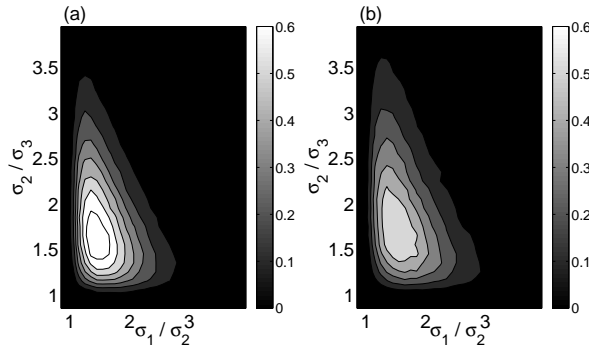


FIG. 17:  $P(\sigma_1/\sigma_2, \sigma_2/\sigma_3)$  for (a) DPPC and (b) sphingomyelin in region 3. The solute radius is  $r = 0.05$  nm. The relative errors are less than ten percent.

that  $\sigma_1$  is the longest axis and  $\sigma_3$  the shortest axis. From these one can extract  $P(\sigma_1/\sigma_2, \sigma_2/\sigma_3)$ , the probability density for finding a with given values of  $\sigma_1/\sigma_2$  and  $\sigma_2/\sigma_3$ . The distribution has been normalized such that integration over it gives unity.

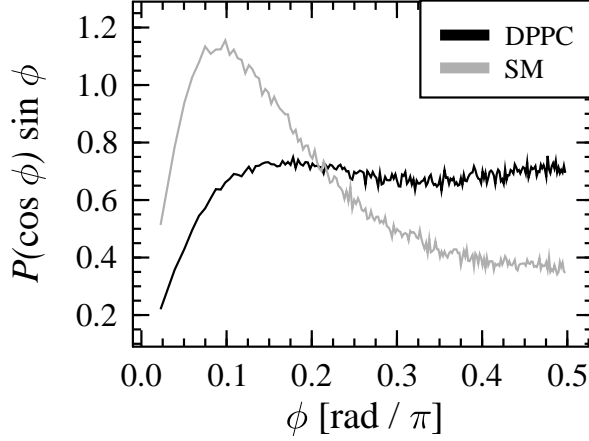


FIG. 18: Orientational distributions  $P(\cos \phi) \sin \phi$  in region 3 for  $r = 0.05$  nm. The relative errors are of the order of five percent.

The behavior of  $P(\sigma_1/\sigma_2, \sigma_2/\sigma_3)$  in region 3 with  $r = 0.05$  nm is portrayed in Fig. 17. We first note that in both DPPC and sphingomyelin elongated voids dominate the distribution; spherical or nearly spherical voids with  $\sigma_1/\sigma_2 \approx \sigma_2/\sigma_3 \approx 1$  are rare. Voids with  $4 \times 10^{-3} \text{ nm}^3 < V < 0.13 \text{ nm}^3$  are a little more elongated in sphingomyelin than in DPPC. This is probably caused by the higher degree of ordering of the sphingomyelin chains. When  $r$  grows, the situation remains very similar to the one depicted in Fig. 17: small and intermediate voids are elongated rather than spherical, and more elongated in sphingomyelin than in DPPC. As for void shape in regions 1, 2, and 4, most voids are elongated and there are very few differences indeed between DPPC and sphingomyelin (data not shown). This appears to be true for all  $r$ .

### C. Void Orientations

PCA also yields the orientations of the principal axes of the ellipsoidal voids with  $4 \times 10^{-3} \text{ nm}^3 < V < 0.13 \text{ nm}^3$ . The quantity  $P(\cos \phi) \sin \phi d\phi$  is the probability that an elongated void is oriented such that the angle between its longest axis and the bilayer normal is between  $\phi$  and  $\phi + d\phi$ , see Ref. 20 for details.

In Fig. 18 we see  $P(\cos \phi) \sin \phi$  in region 3 for  $r = 0.05$  nm. It is clear that DPPC and sphingomyelin differ significantly: orientation along the bilayer normal, or close to it, is much

more common in sphingomyelin than in DPPC. This most likely stems from the fact that the chains are less tilted in sphingomyelin than in DPPC. Increasing  $r$  does not alter the situation (data not shown).

The orientations of small and intermediate voids ( $V < 0.13 \text{ nm}^3$ ) in the other regions have also been considered (data not shown). Orientation in the plane of the bilayer is heavily favored in regions 1 and 2. In these regions the differences between DPPC and sphingomyelin are marginal. As for region 4, the orientations of voids with  $4 \times 10^{-3} \text{ nm}^3 < V < 0.13 \text{ nm}^3$  are quite similar to those in region 3, with similar differences between DPPC and sphingomyelin.

The orientation of voids is expected to play a role in certain physical processes. For example, non-polar fluorescent probes such as diphenylhexatriene (DPH) are commonly used to gauge membrane fluidity (ordering properties) of lipid acyl chains through fluorescence anisotropy measurements.<sup>60,61</sup> While the measurements actually provide insight into the orientation of DPH probes – rather than lipids – in a membrane, it is commonly assumed that the behavior of DPH closely reflects the properties of its local environment in a bilayer, and hence provides information of the ordering of acyl chains, too. Our finding that elongated voids in region 3 are more likely to be oriented along the bilayer normal in PSM than in DPPC is in line with this assumption. Since we expect DPH to fill those voids and to be accommodated in the vicinity of region 3,<sup>60,61</sup> in a PSM bilayer the DPH molecules would have a stronger tendency to be aligned along the bilayer normal. This is consistent with our order parameter results discussed in Sect. IV B, which indicate that PSM is substantially more ordered than DPPC.

## VII. CONCLUDING REMARKS

Biological membranes that surround cells are an example of soft-matter interfaces whose properties can be tuned by weak interactions of the order of thermal energy. The lipid bilayer alone is a fascinatingly complex nanoscale structure: a thin elastic sheet typically about 5 nm thick, consisting of hundreds of different kinds of lipids. The complexity of membranes has been recognized for quite some time, yet their heterogeneous and dynamic nature, as well as their importance in regulating cellular functions has been understood only rather recently. It has been suggested that membranes play a major role for functions governed by membrane proteins; the structure and function of a given membrane protein can be thought to be influenced by the composition of the membrane surrounding the protein. The most recent studies concerning this issue have focused

on unraveling the nature of ordered domains known as lipid rafts<sup>4,5,7,8</sup> rich in a few specific lipids, most notably cholesterol, sphingomyelin, and (almost) saturated phospholipids.

We have investigated the free volume properties of several membrane systems related to rafts. The main motivation for doing so is our view that lipid bilayers are essentially porous thin sheets characterized by a distribution of free volume pockets or voids. The presence of voids is a key to many dynamic processes such as lateral diffusion and permeation. We have considered how the composition of the membrane affects the free volume properties, the emphasis being on those lipids that are commonly found in lipid rafts.

Our data suggest that the amount of free volume is closely coupled to a number of structural and dynamical properties of lipid bilayers. Most significantly, a reduction in free volume is found to correlate with enhanced ordering of acyl chains, a tighter packing of lipid molecules, and reduced area fluctuations. All these are related to the elastic properties of lipid membranes. Our previous studies of phospholipid/cholesterol systems<sup>20</sup> are in line with these findings, and further suggest that there is an interplay between reduced free volume and a slowing down of lateral diffusion.

As for comparison between different lipid systems, we have found that the differences in free volume properties between saturated and diunsaturated phosphatidylcholines are not many. Sphingomyelin, on the other hand, differs significantly from the PCs; in a palmitoylsphingomyelin bilayer the distribution of free area and voids across a membrane is distinctly different from the other cases. Based on the results discussed in the present study and in Ref. 20, it is evident that membranes comprised of large amounts of sphingomyelin and cholesterol, which are the most common lipids found in rafts, are characterized by dense packing, highly ordered acyl chains, and substantially different free volume properties compared to membranes composed of saturated and weakly unsaturated PCs.

The key conclusion is that seemingly minor details in free volume properties may have a large impact on a variety of structural and dynamical characteristics of lipid membranes. While detailed studies of the coupling of free volume with permeation and diffusion of small solutes in the membrane interior are so far missing, there is all reason to assume that similar conclusions are to be expected. As for membrane proteins, it would be fascinating to address the question of the interplay between the composition and free volume properties of a membrane surrounding a protein, the lateral pressure profile around the protein, and the resulting structure of the protein. Work in this direction is in progress.

## VIII. ACKNOWLEDGMENTS

The Wihuri Research Institute is maintained by the Jenny and Antti Wihuri Foundation. This work has, in part, been supported by grants from the Federation of Finnish Insurance Companies, by the Academy of Finland through its Center of Excellence Program (M. Kupiainen, E. F., S. O., P. N., A. G., I. V.), and the Academy of Finland Grant Nos. 80851 (M. H.) 202598 (A. A. G.), and 80246 (I. V.). The Finnish IT Center for Science and the HorseShoe (DCSC) supercluster computing facility at the University of Southern Denmark are thanked for computer resources.

- 
- <sup>1</sup> M. Bloom, E. Evans, and O. G. Mouritsen, *Q. Rev. Biophys.* **24**, 293 (1991).
  - <sup>2</sup> J. Katsaras and T. Gutberlet, eds., *Lipid Bilayers: Structure and Interactions* (Springer-Verlag, Berlin, 2001).
  - <sup>3</sup> M. Edidin, *Nature Reviews Molecular Cell Biology* **4**, 414 (2003).
  - <sup>4</sup> D. A. Brown and E. London, *Annu. Rev. Biophys. Biomol. Struct.* **14**, 111 (1998).
  - <sup>5</sup> M. Edidin, *Annu. Rev. Biophys. Biomol. Struct.* **32**, 257 (2003).
  - <sup>6</sup> S. Mayor and M. Rao, *Traffic* **5**, 231 (2004).
  - <sup>7</sup> K. Simons and W. L. C. Vaz, *Annu. Rev. Biophys. Biomol. Struct.* **33**, 269 (2004).
  - <sup>8</sup> K. Simons and E. Ikonen, *Nature* **387**, 569 (1997).
  - <sup>9</sup> S. J. Marrink, R. M. Sok, and H. J. C. Berendsen, *J. Chem. Phys.* **104**, 9090 (1996).
  - <sup>10</sup> P. F. F. Almeida, W. L. C. Vaz, and T. E. Thompson, *Biochemistry* **31**, 6739 (1992).
  - <sup>11</sup> J. A. Söderhäll and A. Laaksonen, *J. Phys. Chem. B* **105**, 9308 (2001).
  - <sup>12</sup> D. Bassolino-Klimas, H. E. Alper, and T. R. Stouch, *J. Am. Chem. Soc.* **117**, 4118 (1995).
  - <sup>13</sup> D. Bemporad, J. W. Essex, and C. Luttmann, *J. Phys. Chem. B* **108**, 4875 (2004).
  - <sup>14</sup> P. Jedlovsky and M. Mezei, *J. Phys. Chem. B* **107**, 5322 (2003).
  - <sup>15</sup> E. Falck, M. Patra, M. Karttunen, M. T. Hyvönen, and I. Vattulainen, *Biophys. J.* **87**, 1076 (2004).
  - <sup>16</sup> R. S. Cantor, *Biochemistry* **36**, 2339 (1997).
  - <sup>17</sup> R. S. Cantor, *Chem. Phys. Lipids* **101**, 45 (1999).
  - <sup>18</sup> R. S. Cantor, *Biophys. J.* **82**, 2520 (2002).
  - <sup>19</sup> J. Gullingsrud and K. Schulten, *Biophys. J.* **85**, 2087 (2003).
  - <sup>20</sup> E. Falck, M. Patra, M. Karttunen, M. T. Hyvönen, and I. Vattulainen, *J. Chem. Phys.* **121**, 12676 (2004).

- <sup>21</sup> M. G. Alinchenko, A. V. Anikeenko, N. N. Medvedev, V. P. Voloshin, M. Mezei, and P. Jedlovszky, J. Phys. Chem. B **108**, 19056 (2004).
- <sup>22</sup> M. H. Cohen and D. Turnbull, J. Chem. Phys. **31**, 1164 (1959).
- <sup>23</sup> H.-J. Galla, W. H. ann U. Theilen, and E. Sackmann, J. Membrane Biol. **48**, 215 (1979).
- <sup>24</sup> M. E. J. Newman and R. M. Ziff, Phys. Rev. E **64**, 016706 (2001).
- <sup>25</sup> S. Sharma, *Applied Multivariate Techniques* (Wiley, New York, 1996).
- <sup>26</sup> S. J. Marrink and H. J. C. Berendsen, J. Phys. Chem. **98**, 4155 (1994).
- <sup>27</sup> A. Gurtovenko, M. Patra, M. Karttunen, and I. Vattulainen, Biophys. J. **86**, 3461 (2004).
- <sup>28</sup> P. Niemelä, M. T. Hyvönen, and I. Vattulainen, Biophys. J. **87**, 2976 (2004).
- <sup>29</sup> B. Ramstedt and P. Slotte, FEBS Lett. **531**, 33 (2002).
- <sup>30</sup> S. Ollila, M. T. Hyvönen, and I. Vattulainen (2004), to be published.
- <sup>31</sup> E. Lindahl, B. Hess, and D. van der Spoel, J. Mol. Mod. **7**, 306 (2001).
- <sup>32</sup> H. J. C. Berendsen, J. P. M. Postma, W. F. van Gunsteren, A. DiNola, and J. R. Haak, J. Chem. Phys. **81**, 3684 (1984).
- <sup>33</sup> S. Nosé, Mol. Phys. **52**, 255 (1984).
- <sup>34</sup> W. G. Hoover, Phys. Rev. A **31**, 1695 (1985).
- <sup>35</sup> M. Parrinello and A. Rahman, J. Appl. Phys. **52**, 7182 (1981).
- <sup>36</sup> S. Nosé and M. L. Klein, Mol. Phys. **50**, 1055 (1983).
- <sup>37</sup> T. Darden, D. York, and L. Pedersen, J. Chem. Phys. **98**, 10089 (1993).
- <sup>38</sup> U. Essmann, L. Perera, M. L. Berkowitz, T. Darden, H. Lee, and L. G. Pedersen, J. Chem. Phys. **103**, 8577 (1995).
- <sup>39</sup> M. Patra, M. Karttunen, M. T. Hyvönen, E. Falck, P. Lindqvist, and I. Vattulainen, Biophys. J. **84**, 3636 (2003).
- <sup>40</sup> M. Patra, M. Karttunen, M. T. Hyvönen, E. Falck, and I. Vattulainen, J. Phys. Chem. B **108**, 4485 (2004).
- <sup>41</sup> C. Anézo, A. H. de Vries, A.-D. Höltje, D. P. Tieleman, and S.-J. Marrink, J. Phys. Chem. B **107**, 9424 (2003).
- <sup>42</sup> H. J. C. Berendsen, J. P. M. Postma, W. F. van Gunsteren, and J. Hermans, in *Intermolecular Forces*, edited by B. Pullman (Reidel, Dordrecht, 1981), pp. 331–342.
- <sup>43</sup> M. Bachar, P. Brunelle, D. P. Tieleman, and A. Rauk, J. Phys. Chem. B **108**, 7170 (2004).
- <sup>44</sup> J. F. Nagle, R. Zhang, S. Tristram-Nagle, W. Sun, H. I. Petrache, and R. M. Suter, Biophys. J. **70**, 1419 (1996).

- <sup>45</sup> H. I. Petrache, S. W. Dodd, and M. F. Brown, *Biophys. J.* **79**, 3172 (2000).
- <sup>46</sup> S. C. Costigan, P. J. Booth, and R. H. Templer, *Biochim. Biophys. Acta* **1468**, 41 (2000).
- <sup>47</sup> J. F. Nagle and S. Tristam-Nagle, *Biochim. Biophys. Acta* **1469**, 159 (2000).
- <sup>48</sup> P. R. Maulik and G. G. Shipley, *Biochemistry* **35**, 8025 (1996).
- <sup>49</sup> X.-M. Li, J. M. Smaby, M. M. Momsen, H. L. Brockman, and R. E. Brown, *Biophys. J.* **78**, 1921 (2000).
- <sup>50</sup> R. J. Mashl, H. L. Scott, S. Subramaniam, and E. Jakobsson, *Biophys. J.* **81**, 3005 (2001).
- <sup>51</sup> M. T. Hyvönen and P. Kovanen, *Molecular dynamics simulations of unsaturated lipid bilayers: effects of varying the numbers of double bonds* (2005), to appear in the *European Biophysics Journal*.
- <sup>52</sup> C. Huang and J. T. Mason, *Biochim. Biophys. Acta* **864**, 423 (1986).
- <sup>53</sup> I. W. Levin, *Biochemistry* **24**, 6282 (1985).
- <sup>54</sup> Y. Barenholz and T. E. Thompson, *Chem. Phys. Lipids* **102**, 29 (1999).
- <sup>55</sup> P. Niemelä, M. T. Hyvönen, and I. Vattulainen (2005), to be published.
- <sup>56</sup> S. Tristam-Nagle, Y. Liu, J. Legleiter, and J. F. Nagle, *Biophys. J.* **83**, 3324 (2002).
- <sup>57</sup> I. Pascher, M. Lundmark, P. G. Nyholm, and S. Sundell, *Biochim. Biophys. Acta* **1113**, 339 (1992).
- <sup>58</sup> H. I. Petrache, K. Tu, and J. F. Nagle, *Biophys. J.* **76**, 2479 (1999).
- <sup>59</sup> C. Hofsäß, E. Lindahl, and O. Edholm, *Biophys. J.* **84**, 2192 (2003).
- <sup>60</sup> J. Repáková, P. Čapková, J. M. Holopainen, and I. Vattulainen, *J. Phys. Chem. B* **108**, 13438 (2004).
- <sup>61</sup> J. Repáková, J. M. Holopainen, M. R. Morrow, M. C. McDonald, P. Čapková, and I. Vattulainen, *Influence of DPH on the structure and dynamics of a DPPC bilayer* (2005), *Biophys. J.*, in press.
- <sup>62</sup> B. Hoff, E. Strandberg, A. S. Ulrich, D. P. Tieleman, and C. Posten, *Biophys. J.* **88**, 1818 (2005).
- <sup>63</sup> S. Stauffer and A. Aharony, *Introduction to Percolation Theory* (Taylor and Francis, London, 1992), 2nd ed.